Inorg. Chem. **2006**, *45*, 3920–3931

A New Structural Motif for Biological Iron: Iron K-Edge XAS Reveals a $[Fe_4$-μ-$(OR)_5(OR)_{9-10}]$ Cluster in the Ascidian *Perophora annectens*

Patrick Frank,[†,‡] Anthony DeTomaso,[§] Britt Hedman,[‡] and Keith O. Hodgson*[,‡]

Department of Chemistry, Stanford University, Stanford, California 94305-5080, Stanford Synchrotron Radiation Laboratory, SLAC, Stanford University, Stanford, California 94309, and Hopkins Marine Station, Stanford University, Pacific Grove, California 93950-3094

Received August 24, 2005

The Phlebobranch ascidian *Perophora annectens* surprisingly exhibited a biological Fe/V ratio of ∼15:1 on multichannel X-ray fluorescence analysis of two independent collections of organisms. Iron K-edge X-ray absorption spectroscopy (XAS) indicated a single form of iron. The XAS K-edge of the first collection of blood cells was shifted ∼+1 eV relative to that of the second, indicating redox activity with average iron oxidation states of 2.67+ and 2.60+. The first-derivative iron XAS K-edge features at 7120.5, 7124, and 7128 eV resembled the XAS of magnetite but not of ferritin or of dissolved Fe^{II} or Fe^{III}. Pseudo-Voigt fits to blood-cell iron K-edge XAS spectra yielded 12.4 integrated units of preedge intensity, indicating a noncentrosymmetric environment. The non-phase-corrected extended X-ray absorption fine structure (EXAFS) Fourier transform spectrum showed a first-shell O/N peak at 1.55 Å and an intense Fe–Fe feature at 2.65 Å. Fits to the EXAFS required a split first shell with two O at 1.93 Å and three O at 2.07 Å, consistent with terminal and bridging alkoxide ligands, respectively. More distant shells included three C at 2.87 Å, two Fe at 3.08 Å, three O at 3.29 Å, and one Fe at 3.8 Å. Structural models consistent with these findings include a $[Fe_4(OR)_{13}]^{2-/3-}$ broken-edged Fe_4O_5 cuboid or a $[Fe_4(OR)_{14}]^{3-/4-}$ "Jacob's ladder" with three edge-fused $Fe_2(OR)_2$ rhombs. Either of these models represents an entirely new structural motif for biological iron. Vanadium domination of blood-cell metals cannot be a defining trait of Phlebobranch tunicates so long as *P. annectens* is included among them.

Introduction

Perophora annectens, suborder Phlebobranchia, is a colonial tunicate endemic to the temperate waters off the west coast of North America. Individual zooids are ∼1 mm in diameter and are light green, while the colonies share a common vascular system and excurrent siphon.[1] The blood is also light green and under a dissecting microscope is similar in appearance to whole blood from other ascidians.[2−4] *P. annectens* has been reported to sequester up to 5 times more vanadium than the solitary Phlebobranch *Ascidia ceratodes*,[5] which shares a similar East Pacific ecological range.

We were interested in measuring the vanadium K-edge X-ray absorption spectroscopy (XAS) spectra of whole blood from *P. annectens* to compare and contrast them with the results from similar studies on whole blood cells from *A. ceratodes*[6−9] and *Phallusia nigra*.[8,10] *P. annectens* is evolutionarily distant from each of the latter ascidians, and it seemed likely that the biological chemistry of the blood-

* To whom correspondence should be addressed. E-mail: Hodgson@ssrl.slac.stanford.edu. Tel: 650-926-3153.
† Department of Chemistry.
‡ Stanford Synchrotron Radiation Laboratory, SLAC.
§ Hopkins Marine Station.

(1) Morris, R. H.; Abbott, D. P.; Haderlie, E. C. *Intertidal Invertebrates of California*; Stanford University Press: Stanford, 1980.
(2) George, W. C. *J. Morph. Physiol.* **1930**, *49*, 385−413.
(3) George, W. C. *Quart. J. Microsc. Sci.* **1939**, *81*, 391−430.
(4) Wright, R. K. Urochordates. In *Invertebrate Blood Cells*; Ratcliffe, N. A., Rowley, A. F., Eds.; Academic Press: London, 1981; Vol. 2, pp 565−626.
(5) Swinehart, J. H.; Biggs, W. R.; Halko, D. J.; Schroeder, N. C. *Biol. Bull.* **1974**, *146*, 302−312.
(6) Frank, P.; Kustin, K.; Robinson, W. E.; Linebaugh, L.; Hodgson, K. O. *Inorg. Chem.* **1995**, *34*, 5942−5949.
(7) Frank, P.; Hodgson, K. O. *Inorg. Chem.* **2000**, *39*, 6018−6027.
(8) Frank, P.; Robinson, W. E.; Kustin, K.; Hodgson, K. O. *J. Inorg. Biochem.* **2001**, *86*, 635−648.
(9) Frank, P.; Carlson, R. M. K.; Carlson, E. J.; Hodgson, K. O. *J. Inorg. Biochem.* **2003**, *94*, 59−71.
(10) Frank, P.; Hodgson, K. O.; Kustin, K.; Robinson, W. E. *J. Biol. Chem.* **1998**, *38*, 24498−24503.

10.1021/ic051445x CCC: $33.50
Published on Web 04/21/2006

cell vanadium would reflect this distance. Surprisingly, XAS examination of independent *P. annectens* whole-body and whole-blood-cell samples revealed little vanadium but copious iron. Here we report the first X-ray spectroscopic study of iron-bearing ascidian blood cells.

Materials and Methods

Two separate collections of *P. annectens* were obtained. The first *P. annectens* collection (collection 1) was taken from the tidally flushed base of the Monterey Bay Aquarium, Monterey, CA (36° 37.067′ N; 121° 54.10′ W). The second collection (collection 2) was obtained from the nearby Hopkins Marine Station within the Pacific Grove Marine Biological Refuge in Monterey Bay, CA (36° 37.366′ N; 121° 53.988′ W; subtidal collection depth 75 ft). From these collections, a total of four XAS samples were obtained. From collection 1, these included two whole-blood samples, plus one whole-body sample. From collection 2, only a single whole-body sample was obtained.

For XAS sample preparation, as-collected zooids were immersed in seawater under a dissecting microscope. Single *P. annectens* were then removed from their substratum using a pair of fine-point tweezers. The green individual specimens of *P. annectens* were observed to be free of extraneous solids.

For the two whole-blood-cell samples from collection 1, groups of freed individual zooids were gathered and pressed against a 100-μm nylon mesh net. The emergent whole blood was collected within a cold conical glass tube. When sufficient settled blood-cell volume was obtained, the collected light-green blood was transferred into a Lexan XAS sample cell and frozen immediately in liquid nitrogen.

Two whole-body samples were also obtained, one each from collections 1 and 2. Thus, individual zooids, freed as above, were transferred directly into a Lexan XAS sample cell, which was then frozen in liquid nitrogen. All samples were stored under liquid nitrogen until XAS measurement.

For metal analysis of a tidal water sample, 899.98 g of water, near the base of the Monterey Bay Aquarium and next to the collection 1 *P. annectens* colony, was collected in an acid (HCl)-washed plastic bottle. The density of the Monterey Bay tidal water sample was measured at ambient temperature using a (10.00 ± 0.04)-mL class A volumetric flask and a Mettler semi-micro analytical balance, yielding $d = 1.018 \pm 0.004$ g/mL. For metal analysis, the water was shell-frozen and lyophilized to yield 38.72 g of dry solids, which were ground to a fine powder using a quartz pestle. The solids were analyzed in duplicate for the total vanadium and iron by the method of inductively coupled plasma fluorescence emission spectroscopy (Galbraith Laboratories, Knoxville, TN), yielding 38 ± 1 ppm Fe and 2.1 ± 0.4 ppm V.

Iron model solutions were prepared within a glovebox (Vacuum Atmospheres, Hawthorne, CA) operating at ≤1 ppm O_2. Anhydrous $FeCl_2$ (Aldrich Chemicals, 99.998%) or $FeCl_3$ (Fisher Scientific, purified grade) was dissolved in 1 M HCl to yield 100 mM stock solutions of iron. The solution of ferrous chloride was colorless. These were diluted 10-fold with 1 M HCl to prepare the XAS samples of $[Fe(aq)]^{2+}$ or $[Fe(aq)]^{3+}$. Solution samples of the iron ethylenediaminetetraacetic acid (EDTA) complexes were made by diluting the above stock iron solutions with appropriate volumes of 20 mM Na_2H_2EDTA in 25 mM TrisHCl (pH 7.4) to yield a 2-fold excess of ligand. The solution of $[Fe(EDTA)]^{2-}$ was adjusted to pH 8.2 with solid KOH. Likewise, the $[Fe(EDTA)]^{-}$ solution was adjusted to pH 8.1. Iron K-edge XAS spectra of authentic magnetite and holoferritin were kindly supplied by Prof. Helen Nichol, Department of Anatomy and Cell Biology, University of Saskatchewan, Saskatoon, Saskatchewan, Canada.

XAS spectra were measured at SSRL on unfocused wiggler beamline 7-3 under dedicated operating conditions of 3 GeV and 68−86-mA current and with an 18-kG wiggler field. The incident X-ray beam was energy-discriminated using a Si[220] double-crystal monochromator, which was detuned 50% at 7987 eV to minimize harmonic contamination. Multichannel analyzer (MCA) traces were measured as fluorescence following irradiation of *P. annectens* samples at 8000 or 10 000 eV. Iron K-edge XAS spectra were measured in fluorescence mode using a Canberra 30-element array germanium detector. All XAS samples were held at 5.6 K using an Oxford Instruments CF1208 continuous-flow liquid-helium cryostat. Iron foil calibration spectra were concurrently measured as transmission XAS using an in-line nitrogen-filled ionization chamber as the detector. The *P. annectens* XAS spectra were calibrated to the first inflection of the rising edge of the iron foil X-ray spectrum, set at 7111.30 eV, and processed using the same method as that described previously in detail for XAS data obtained on vanadium-containing blood-cell samples from *A. ceratodes*.[6,7] The EXAFS spectra are the sum of four scans obtained on whole-blood-cell sample 1. The fluorescent X-ray emission spectra were obtained using a Canberra 30-element array germanium detector, with 4096 MCA channels.

The *P. annectens* iron K-edge EXAFS data were fit using the EXAFSPAK package of data-processing software written by Dr. Graham George (Department of Geological Sciences, University of Saskatchewan, Saskatoon, Saskatchewan, Canada), with theoretical phase and amplitude functions calculated using FEFF 7,[11,12] based on initial structural models derived from known structures. EXAFSPAK is available free of charge at the SSRL Web site http://www-ssrl.slac.stanford.edu/~xas/xas-software.html. The data were fit over the k range 2−11 Å^{-1}, with ice-crystal diffraction spikes in the data setting the higher k limit. In the fits to EXAFS data, coordination numbers were generally fixed at integer or half-integer values, while absorber−scatterer distances and Debye−Waller (DW) values were allowed to float. The values for E_0 were also floated but were linked and were required to vary as a group and refine to a common value. The total number of parameters floated during a fit was therefore $2n + 1$, where n is the number of scatterer shells. The total number of independent points, N_I, in an EXAFS fit is given by $N_I = (2\delta k \times \delta R/\pi) + 2$,[13] where δk is the range of photoelectron wave vector containing usable EXAFS data and δR is either the width of the Fourier transform (FT) region containing the fitted features or the R range of back-transformed fitted EXAFS data. In the fits reported herein, the fitted non-phase-corrected FT data occupied the range between 0.6 and 3.6 Å. The integer value of N_I therefore was 19, while the maximum number of floated variables never exceeded 13 in any fit. The final fit included 13 floated variables, and the EXAFS data were thus not overfitted. The uncertainty in absorber−scatterer distances was obtained from the statistical errors calculated by the final fit.

The pseudo-Voigt fits to iron K-edge XAS spectra were carried out using the program Edg_Fit, which is also part of the EXAFSPAK data-analysis package. Pseudo-Voigt lines are the sum of Gaussian and Lorentzian functions, and the ratio of these lines was fixed at 1:1 in the described fits. The half-widths at half-height of the component pseudo-Voigt lines were typically linked and forced to refine together as a common value. The pseudo-Voigt half-widths were also required to be no more than 1.0 eV greater

(11) Rehr, J. J.; Mustre de Leon, J.; Zabinsky, S. I.; Albers, R. C. *J. Am. Chem. Soc.* **1991**, *113*, 5135−5140.
(12) Zabinsky, S. I.; Rehr, J. J.; Ankudinov, A.; Albers, R. C.; Eller, M. J. *Phys. Rev. B* **1995**, *52*, 2995−3009.
(13) Stern, E. A. *Phys. Rev. B* **1993**, *48*, 9825−9827.

than the natural 1.25-eV core-hole lifetime width of iron.[14] Finally, a fit was deemed acceptable if it reproduced both the K-edge XAS spectrum and the first derivative of the XAS spectrum to within the limits of the spectral noise. Gaussian fits to the MCA spectra also utilized the Edg_Fit program. The half-widths at half-height were again linked and refined together, with the only exception being that of the excitation line at 8000 or 10 000 eV, which was allowed to float separately.

Results

K-edge XAS spectra were obtained from four *P. annectens* samples, including two whole-blood samples and one whole-body sample from the first collection of specimens and one whole-body sample from the second collection (see the Materials and Methods section for the collection details). Usable EXAFS data were obtained from one whole-blood sample. The initial vanadium K-edge XAS spectrum, obtained from the better of two *P. annectens* collection 1 whole-blood samples, showed a very poor signal-to-noise ratio indicative of a very low concentration of this metal. This was surprising in light of previously reported *P. annectens* blood vanadium concentrations of up to 9000 ppm.[5,15] To more fully investigate the metal content of this sample, we carried out an X-ray fluorescence MCA measurement using a high-energy-resolution germanium solid-state detector array. Multielement MCA fluorescence emission spectra involve X-ray irradiation of the sample at energies greater than the 1s core ionization potentials of the elements of interest. Absorption of an X-ray by each element present is followed by photoejection of a core electron. The subsequent cascade of electrons from higher-energy orbitals into the empty core state produces a characteristic X-ray fluorescence emission spectrum. For transition metals, the highest-energy np $\rightarrow$ 1s transitions produce intense Kα and Kβ X-ray fluorescence emission lines that represent electronic transitions from 2p and 3p states, respectively, and occur at energies diagnostic of each element. Figure 1 shows the results from MCA experiments on separate samples consisting of *P. annectens* whole bodies and whole blood, respectively, using an 8-keV excitation energy.

In the MCA spectra of Figure 1, the Kα line for vanadium (4945 eV) is only just visible above the baseline, indicating a low concentration of this metal and explaining the extremely weak vanadium K-edge exhibited by the *P. annectens* blood-cell sample. However, the Kα emission from iron (6391 eV) is very intense and completely dwarfs the vanadium Kα line. These results held true for the MCA spectra of all four *P. annectens* samples representing two separate collections that were obtained either from the tidal zone or subtidally and collected months apart. Gaussian fits to all of the MCA spectra (Figure 1, inset) allowed estimation of the biological metal ratios, assuming comparable intrinsic K-shell fluorescence intensities (see below). The integrated intensities of the fitted Gaussians yielded V/Fe ratios of about

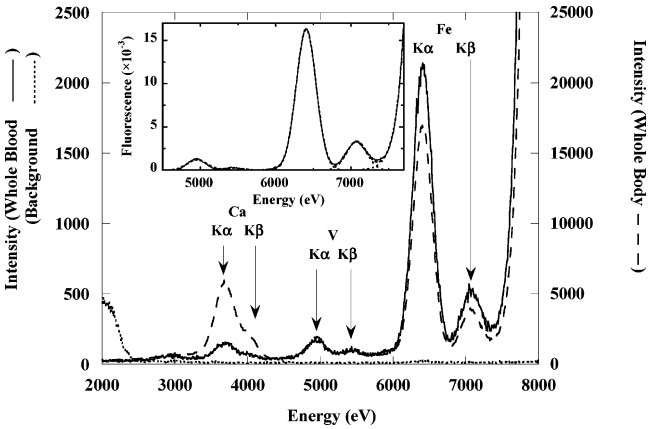

Figure 1. MCA traces of (left ordinate) (···) the cryostat background and (—) a sample of whole blood cells and (right ordinate) (- - -) whole bodies of *P. annectens*. The X-ray irradiation energy was 8 keV. Inset: (—) the whole-body MCA spectrum, (- - -) the Gaussian fit, and (···) the individual Gaussian components.

1:11 and 1:16 in the two whole-blood-cell samples of collection 1 and V/Fe ratios of about 1:14 and 1:17 in the independent whole-body samples from collections 1 and 2, respectively.

Using an excitation energy of 10 keV, the MCA spectrum of the whole-body sample from collection 2 showed two further strong emission lines at higher energies (Figure 1 in the Supporting Information), consistent with significant concentrations of biological copper and zinc. The Gaussian fit to this MCA spectrum (Figure 1, inset, in the Supporting Information) allowed an estimation of the Fe/Zn/Cu/V metal ratios in that sample, which were 17:5:1.6:1. The metal ratios were not corrected for the small errors introduced by the systematic decrease in the K-shell X-ray fluorescence intensity, which is due to the diminishing absorption cross section as the excitation X-ray photon trends to higher energy than the relevant K-shell ionization potential.[16]

The tidally flushed area where the collection 1 *P. annectens* samples were taken included some rusting steel bars, and it seemed possible that the surprising reversal of iron and vanadium in these organisms could be a local adaptation to a high ambient iron concentration. In part for this reason, the second collection of *P. annectens* was taken from a well-removed and pristine locale (collection 2; see the Materials and Methods section). A sample of the tidally flushed water near the collection 1 colony of *P. annectens* was acquired and analyzed for iron and vanadium, yielding [Fe] = 1.6 ppm and [V] = 90 ppb. In 1990, the iron content of Monterey Bay water was found to be 71 ppb,[17] compared to about 1.1−27 ppb in North Pacific surface waters.[18] For vanadium, the North Pacific surface concentration is about 1.6 ppb, but no estimate of the average Monterey Bay [V] is currently available. It is clear that iron is generally enriched in

(14) Krause, M. O.; Oliver, H. H. *J. Phys. Chem. Ref. Data* **1979**, *8*, 329−338.
(15) Ciereszko, L. S.; Ciereszko, E. M.; Harris, E. R.; Lane, C. A. *Comp. Biochem. Physiol.* **1963**, *8*, 137−140.
(16) Agarwal, B. K. *X-ray Spectroscopy*; Springer-Verlag: Berlin; 1979; Vol. 15, p 63ff.
(17) Phillips, R. Influent Water Elemental Analysis, Monterey Bay Aquarium, Monterey, CA, Aug 2, 1990; American Analytical Laboratories, Report No. 034931, Sept 17, 1990.
(18) Donat, J. R.; Bruland, K. W. Trace Elements in the Ocean. In *Trace Elements in Natural Waters*; Salbu, B., Steinnes, E., Eds.; CRC Press: Boca Raton, FL, 1995; pp 247−281.

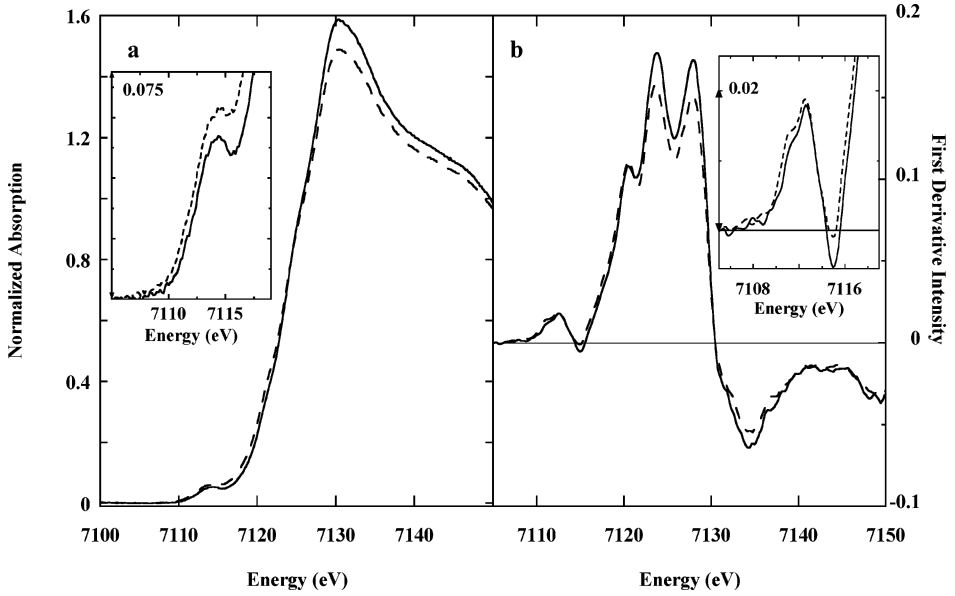

Figure 2. Iron K-edge XAS spectra. Part a: (—) whole blood cells and (- - -) whole bodies of *P. annectens*. Inset: expansion of the preedge energy region showing the 1s → 3d transition manifold. Part b: first derivatives of the spectra in part a.

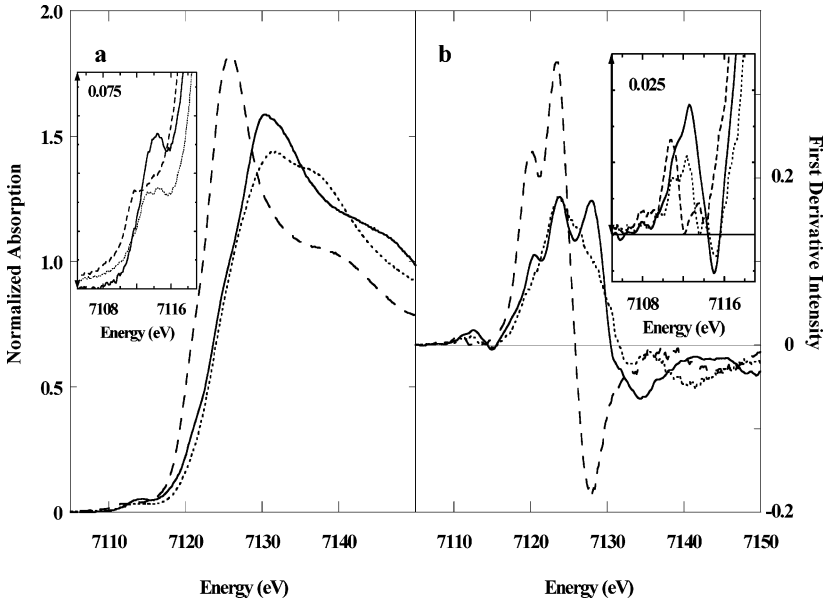

Figure 3. Iron K-edge XAS spectra. Part a: (—) *P. annectens* whole blood cells, (- - -) $FeCl_2$, 9.9 mM in a 1 M HCl solution, and (···) $FeCl_3$, 9.9 mM in a 1 M HCl solution. Inset: expansion of the preedge energy region. Part b: first derivatives of the XAS spectra in part a. Inset: first derivatives of the preedge spectra in the part a inset.

Monterey Bay waters compared to the open ocean. However, the tidal water near the site of collection 1 was even more highly enriched in iron, as suspected. Nevertheless, despite the apparent nearly 22.5-fold difference in ambient aqueous iron of the two Monterey Bay locations, the collection 1 and 2 whole-body samples gave very similar ~15:1 Fe/V ratios. This finding indicated a consistent biological regulation in the face of varying exposure to external metals. Therefore, the high iron content found in *P. annectens* is not an artifact of the locally high available [Fe].

The iron K-edge XAS spectra of the collection 1 *P. annectens* whole-body and whole-blood-cell samples are displayed in Figure 2a. Figure 2b shows the first derivatives of these XAS spectra. The high signal-to-noise ratios show that considerable iron is present in both samples. The same form of iron predominates in both samples, and thus the metallobiochemistry of *P. annectens* largely consists of a single suite of iron. The general oxidation state of *P. annectens* iron can be evaluated by a comparison of the XAS rising-edge maximum with the XAS spectra of solution $FeCl_3$ ($[Fe(aq)]^{3+}$) and $FeCl_2$ ($[Fe(aq)]^{2+}$), shown in Figure 3. These values, 7130.5, 7131.5, and 7125.8 eV, respectively, establish that the iron in *P. annectens* blood cells is close to Fe^{III} but with a somewhat lower effective nuclear charge, Z_{eff}.[19] However, the shape of the rising XAS K-edge of *P. annectens* blood cells is very dissimilar from that of $[Fe(aq)]^{3+}$, showing that the blood cells do not contain dissolved aqueous Fe^{III} in an acidic solution or a mixture of dissolved

(19) Westre, T. E.; Kennepohl, P.; DeWitt, J. G.; Hedman, B.; Hodgson, K. O.; Solomon, E. I. *J. Am. Chem. Soc.* **1997**, *119*, 6297−6314.

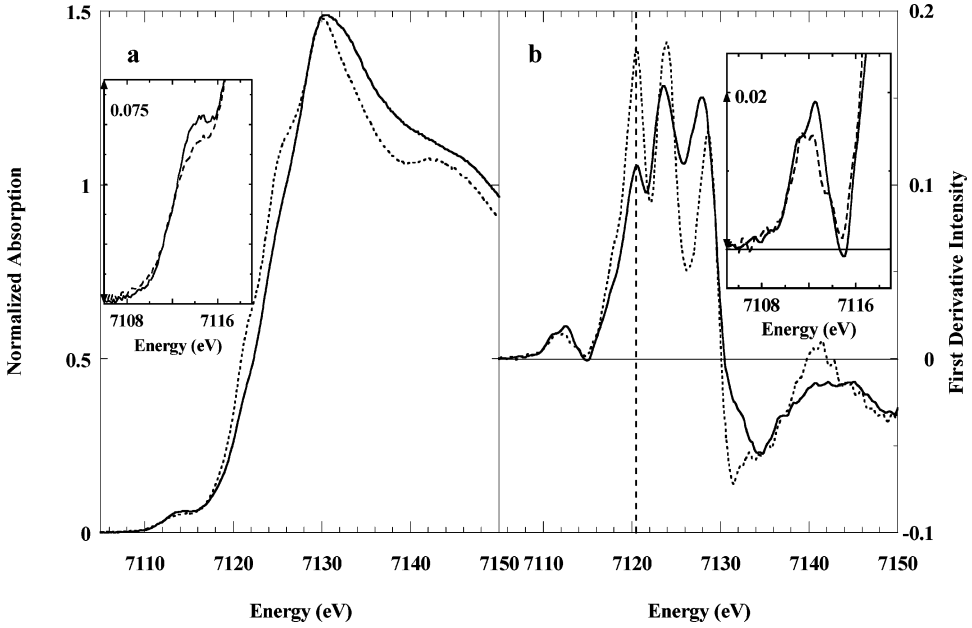

Figure 4. Iron K-edge XAS spectra of *P. annectens* whole bodies. Part a: (—) collection 1 and (- - -) collection 2. Inset: expansion of the preedge energy region of the XAS spectra. Part b: first derivatives of the XAS spectra of part a. Inset: first derivatives of the preedge spectra of the inset in part a. The vertical line marks 7120.5 eV.

aquated ferrous and ferric ions. Thus, the iron in *P. annectens* is not analogous to the solution of vanadium(III) sulfate in aqueous sulfuric acid that predominates in the blood cells of the vanadium-accumulating Phlebobranch tunicates *A. ceratodes*,[6,8,20] *A. gemmata*, *A. ahodori*, and *A. sydneiensis samea*[21−23] and likely in *A. obliqua* and *Ph. mammillata*,[24,25] and *Ascidiella aspersa*.[26]

In the preedge energy region, the Figure 3a inset shows that the 1s → 3d transition of *P. annectens* iron is noticeably more intense than those of the aqua ions, implying a lower-symmetry iron ligation environment. The intensity of the preedge feature was evaluated by carrying out a pseudo-Voigt fit to the whole-blood XAS spectrum over the energy range 7105−7150 eV. This fit (Figures 2 and 3 in the Supporting Information) gave an integrated intensity of 12.4 normalized units for the preedge feature, a value consistent with the absence of centrosymmetry about the iron.[19,27,28]

Figure 4 shows that the iron K-edge XAS spectra of *P. annectens* whole-body collections 1 and 2 exhibit comparative differences that could reflect redox activity. The absorption maximum of the collection 1 whole-body iron K-edge XAS spectrum (7130.7 eV) is 0.5 eV higher in energy than the iron XAS maximum of collection 2 (7130.2 eV). The rising K-edge of the collection 1 sample is also shifted by about 1 eV to higher energy, and the shoulders on the rising edge are also far less prominent. However, the first derivatives of the XAS spectra in Figure 4b show that the first rising-edge transitions occur at the same energy despite the difference in the intensity. The subsequent two first-derivative features in the collection 2 XAS spectrum have shifted to *higher* energy by 0.5 and 0.6 eV, respectively, in contrast to the trend in XAS absorption maxima. The preedge transition of the collection 2 XAS spectrum shows a distinct loss of intensity (Figure 4a, inset). These results are consistent with partial reduction of the biological iron in the collection 2 whole-body sample relative to collection 1[19,27−29] and will be discussed further below. Pseudo-Voigt fits to the collection 1 and 2 whole-body XAS spectra yielded preedge intensities of 18.5 and 12.5 normalized units, respectively. These values quantify the perceived lower intensity of the preedge XAS features of the collection 2 sample and are again consistent with a lack of centrosymmetry in the iron environment within each sample.

To further characterize the Fe site, *P. annectens* iron K-edge XAS spectra were compared with a series of iron-containing models, including magnetite and the biological iron in ferritin (Figure 5). Ferritin is an iron-storage protein containing an iron oxo−hydroxo core most similar in structure to the iron(III) mineral ferrihydrite, $5Fe_2O_3 \cdot 5H_2O$, and is ubiquitous in organismal biology from bacteria to mammals.[30,31] Magnetite, Fe_3O_4, is a widespread geological Fe^{II}/Fe^{III} mineral but is also found in bacterial through

(20) Frank, P.; Carlson, R. M. K.; Hodgson, K. O. *Inorg. Chem.* **1986**, *25*, 470−478.
(21) Michibata, H.; Hirata, J.; Uesaka, M.; Numakunai, T.; Sakurai, H. *J. Exp. Zool.* **1987**, *244*, 33−38.
(22) Michibata, H.; Iwata, Y.; Hirata, J. *J. Exp. Zool.* **1991**, *257*, 306−313.
(23) Kanamori, K.; Michibata, H. *Mar. Biol. Assoc.* **1994**, *74*, 279−286.
(24) Boeri, E.; Eherenberg, A. *Arch. Biochem. Biophys.* **1954**, *50*, 404−416.
(25) Bielig, H.-J.; Bayer, E.; Dell, H.-D.; Rohns, G.; Möllinger, H.; Rüdinger, W. *Protides Biol. Fluids* **1966**, *14*, 197−204.
(26) Rezaeva, L. T. *Zh. Obsch. Biol.* **1964**, *25*, 347 (T836−T840).
(27) Roe, A. L.; Schneider, D. J.; Mayer, R. J.; Pyrz, J. W.; Widom, J.; Que, L., Jr. *J. Am. Chem. Soc.* **1984**, *106*, 1676−1681.
(28) Randall, C. R.; Shu, L.; Chiou, Y.-M.; Hagen, K. S.; Ito, M.; Kitajima, N.; Lachicotte, R. J.; Zang, Y.; Que, L., Jr. *Inorg. Chem.* **1995**, *34*, 1036−1039.
(29) Wilke, M.; Farges, F.; Petit, P. E.; Brown, G. E., Jr.; Martin, F. *Am. Mineral.* **2001**, *86*, 714−730.
(30) Aisen, P.; Enns, C.; Wessling-Resnick, M. *Int. J. Biochem. Cell Biol.* **2001**, *33*, 940−959.
(31) Arosio, P.; Levi, S. *Free Radicals Chem., Biol. Med.* **2002**, *33*, 457−463.

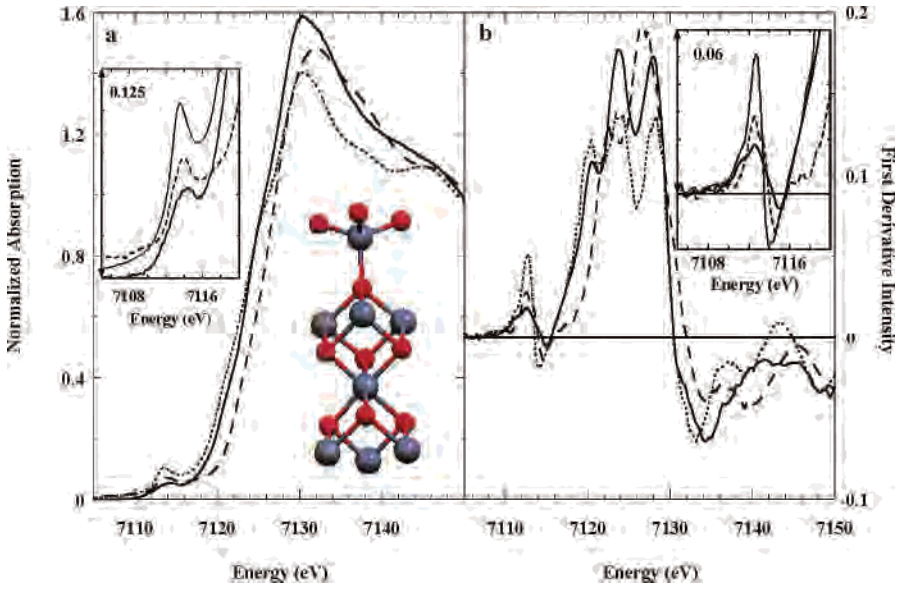

Figure 5. Iron K-edge XAS spectra (a) and first derivatives of the XAS data (b) of (—) *P. annectens* whole blood cells, (- - -) ferritin, and (···) magnetite. The insets show an expansion of the preedge region of the XAS spectra. The structural inset of part a shows the repeating cubic motif of magnetite. The dark spheres represent Fe atoms, and the lighter spheres represent O atoms.

mammalian cells as 50−100-nm crystals that are typically not associated with a discrete protein binding site.[32−34] Figure 5a shows that the absorption maximum of ferritin Fe^{III} at 7132.0 eV is more than 1.5 eV higher in energy than that of either magnetite or *P. annectens* iron, which are virtually coincident at 7130.5 eV. The first derivative of the *P. annectens* iron XAS is also strikingly similar to that of magnetite, including similar features near 7120.5, 7123.8, and 7128 eV.

The iron XAS spectrum of none of the other mononuclear iron models examined exhibited this sort of resemblance. Thus, an analogous similarity of the structure in the iron of magnetite and *P. annectens* was inferred. The structure of magnetite,[35] inset to Figure 5a, includes a repeating Fe_4O_4 cube. Magnetite is a 2:1 Fe^{III}/Fe^{II} mixed-valent mineral, and the coincidence in the XAS energy maximum with that of *P.* annectens implies magnetite and *P. annectens* iron have the same average formal oxidation state ($Fe^{2.67+}$). To test this idea, a numerically generated spectrum of oxo-bridged $Fe^{2.67+}$ was prepared by the ratioed addition of the iron K-edge XAS spectra of fully oxidized and fully reduced methane monooxygenase (MMO),[36] which contains a μ-di-oxo-bridged non-heme iron dimer. The energy positions of both the rising edge and the absorption maximum of this $Fe^{2.67+}$ XAS addition spectrum were virtually coincident with the XAS of collection 1 *P. annectens* blood-cell iron (Figure 4 in the Supporting Information).

Despite the presence of crystalline ice, we were able to measure iron K-edge EXAFS spectra from the collection 1 blood-cell sample, which was usable over the range $k = 2-11$ Å^{-1}. The phase-shift-uncorrected FT of these data is shown in Figure 6. Two intense features are observed, with

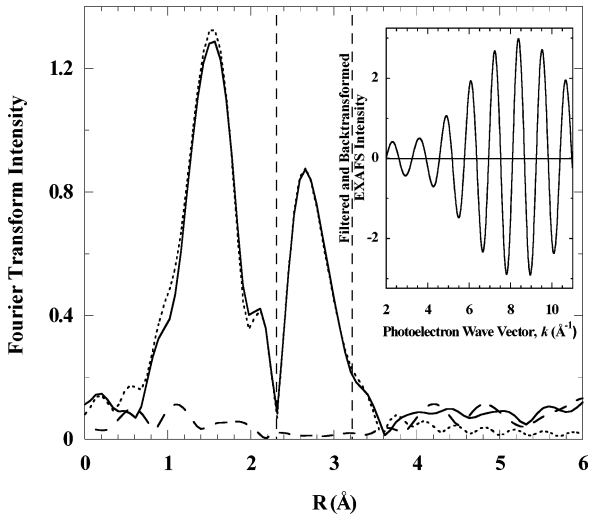

Figure 6. Iron K-edge FT EXAFS of (—) *P. annectens* whole blood, (- - -) the fit to the EXAFS, and (- - -) the data minus the fit residual. The data are not phase-shift-corrected. The vertical dashed lines indicate the 2.3−3.2 range in *R* over which the second-shell peak at 2.65 Å was windowed and back-transformed. The inset shows the back-transformed EXAFS of the second-shell FT peak.

the first peak at 1.55 Å identifiable as first-shell O/N scatterers. The second feature at 2.65 Å is too distant to represent first-shell ligation by a heavier ligand such as sulfur. Back-transformation of this feature (Figure 6, inset) produced a single EXAFS wave with an amplitude maximum at $k = 8.4$ Å^{-1}, consistent with a second-shell high-*Z* transition-metal scatterer. The intensity of the second-shell (2.65 Å) FT peak compared to the first-shell peak is 0.67 and is energy-shifted and much weaker than the second-shell FT EXAFS peak of the iron-containing minerals magnetite (Fe_3O_4) and goethite [Fe(O)OH] (see below),[37] obviating a mineral contaminant.

(32) Šafarík, I.; Šafaríková, M. *Monatsh. Chem.* **2002**, *133*, 737−759.
(33) Matsunaga, T.; Okamura, Y. *Trends Microbiol.* **2003**, *11*, 536−541.
(34) Schuler, D. *Arch. Microbiol.* **2004**, *181*, 1−7.
(35) Fleet, M. E. *Acta Crystallogr.* **1982**, *B37*, 917−920.
(36) DeWitt, J. G.; Bentsen, J. G.; Rosenzweig, A. C.; Hedman, B.; Green, J.; Pilkington, S.; Papaefthymiou, G. C.; Dalton, H.; Hodgson, K. O.; Lippard, S. J. *J. Am. Chem. Soc.* **1991**, *113*, 9219−9235.

Fits to the EXAFS data thus took the simplest approach to modeling the high-*Z* second-shell scatterer, assigning it to Fe. The first shell was represented as O atoms, although EXAFS fitting cannot distinguish between O and N backscatterers. However, the distinct lack of the FT features of distant-shell imidazole C atoms above 3 Å almost certainly excludes histidine ligation.

A first-shell iron coordination number of 6 produced an excessively large DW factor ($\sigma^2 = 0.0105$), and the position of the fitted first-shell FT peak was offset by about −0.05 Å from the data peak. The fits obtained with five first-shell scatterers remained offset in *R*, and the DW value, though reduced, remained relatively high (e.g., $\sigma^2 = 0.0083$). Splitting the first shell into three 1.93 Å plus three 2.07 Å O/N atoms produced unacceptably high DW values for the first shell (e.g., $\sigma^2 = 0.01475$) but a better fit to the FT peak position. Much more acceptable fits were obtained when the first shell was split into two 1.93 Å plus three 2.07 Å O/N atoms. The DW values were reduced to acceptable levels, and the FT peak of the fit coincided with the main FT data peak. Although the 0.14-Å difference in first-shell distances is somewhat smaller than the resolution allowed by data (0.18 Å), the improvements in the fit and DW values were so marked that two first-shell distances were carried through the fits.

When only one distant Fe was used to fit the second-shell FT peak, negative or very small DW values were obtained. This was taken to indicate that the average Fe atom sees at least two distant Fe scatterers. Subsequent fits therefore investigated a series of models including two or three distant Fe scatterers, making a total of three to four Fe atoms in the *P. annectens* iron complex. Likewise, the shoulder in the FT spectrum at 2.11 Å was well-fit with second-shell C scatterers. With the addition of C, the models tested in the EXAFS fits were generally defined as having oxo or alkoxido bridges and alkoxido terminal ligands and included linear, three-Fe-center chains, $Fe_3O_3(OR)_6$ metallocyclohexanes, $Fe_3O_4(OR)_6$ open cubes, and $Fe_4O_4(OR)_8$ closed cubes. These were varied where appropriate with one or two bridging O atoms between Fe atoms and with the number of second-shell C atoms varied to account for the oxo or alkoxido identities of the different ligands.

However, fits to the data with two first-shell O waves and two or three Fe waves plus a second shell of C waves did not fully reproduce the second-shell 2.65-Å FT feature, in that the intensity was overestimated and the entire high-*R* side of the peak was left unfit (Figure 5 in the Supporting Information). In addition, the fit to the first-shell peak was not completely satisfactory. The FT was therefore back-transformed in the region between 3.2 and 3.6 Å. The filtered back-transformed EXAFS spectrum, shown in Figure 6 in the Supporting Information, exhibited an amplitude envelope with a maximum near $k = 10$ Å^{-1}, consistent with a distant metal scatterer. Thus, adding a shell of one Fe at 3.4 Å greatly improved the fit to the second-shell FT feature, decreasing the *F* value from 0.2804 to 0.2530. Alternatively, adding a shell of three distant O atoms at about 3.3 Å also improved the fit to this region of the FT spectrum, lowering *F* from 0.2804 to 0.2523. The FTs of these intermediate fits are compared with data in Figure 5 in the Supporting Information. In the event, however, the second-shell Fe feature and the shoulder at 3.4 Å in the FT spectrum were fully fit only with the addition of both distant shells. This addition also improved the fit to the first-shell feature and to the mostly C shoulder at 2.11 Å and dropped the goodness-of-fit *F* to 0.2476.

Nonetheless, the 3.8-Å Fe scatterer does not contribute a large feature to the FT spectrum. Therefore, we further tested the need for the 3.8-Å Fe by substituting distant alternative lower *Z* scatterers. The results of these tests are shown in Figures 5 and 7 and Table 1 in the Supporting Information. In short, neither additional C atoms nor additional O atoms alone were able to adequately fit the 3.4-Å FT feature, including multiple O waves representing 3.8-Å scatterers. These results show that the amplitude envelope of the 3.4-Å FT feature, as implied by the back-transformation described above and shown in Figure 6 in the Supporting Information, indeed signified a distant metal scatterer. The integer number of independent points, N_I, in the second-shell FT feature is 9 (see the Materials and Methods section), while the final fit using two Fe shells plus the 3.3-Å O shell included seven floated variables. Therefore, adding the 3.8-Å Fe shell did not overfit the data in the second FT peak.

Finally, regular Fe_4O_4 cubane models were also tested to see whether the 3.8-Å Fe shell could be eliminated. These models included three Fe scatterers at about 3.1 Å, a C shell at ∼2.86 Å, and a distant O shell at ∼3.3 Å. However, these fits did not reproduce the high-*R* region of the FT of the EXAFS data as well as the model containing the 3.8-Å Fe shell. Splitting the 3.1-Å Fe shell in the Fe_4O_4 model yielded two Fe scatterers at 3.07 Å and one Fe scatterer at 2.85 Å ($F = 0.2464$). However, despite the slightly improved *F* value, this fit also did not model the high-*R* FT feature as well as the final fit. These fits are shown in Figure 8 in the Supporting Information. Splitting the 3.08-Å Fe shell improved the final fit as well ($F = 0.2446$) but added no new constraints on the structural hypothesis.

The possibility of a heterometal site is established by the detection of organismal Cu and Zn in the MCA experiment (Figure 1 in the Supporting Information). However, the 11:1 ratio of Fe/Cu excludes the latter metal from contributing any appreciable portion of a four-site metal cluster. The measured ratio of Fe/Zn, 3.4:1, makes an Fe_3Zn cluster possible within the limits of the MCA measurement. The uniqueness of the all-Fe model was tested using a structural model in which Cu or Zn were substituted into Fe sites. Equally good fits were found with either a distant Cu ($F = 0.2471$) or Zn ($F = 0.2456$) scatterer. Therefore, the possibility of an Fe_3Zn heterometal cluster cannot be strictly eliminated without measuring the Zn EXAFS of *P. annectens* blood cells. In light of the discussion immediately preceding, however, we also note that the successful fit including a

(37) Heath, S. L.; Charnock, J. M.; Garner, C. D.; Powell, A. K. *Chem.—Eur. J.* **1996**, *2*, 634−639.

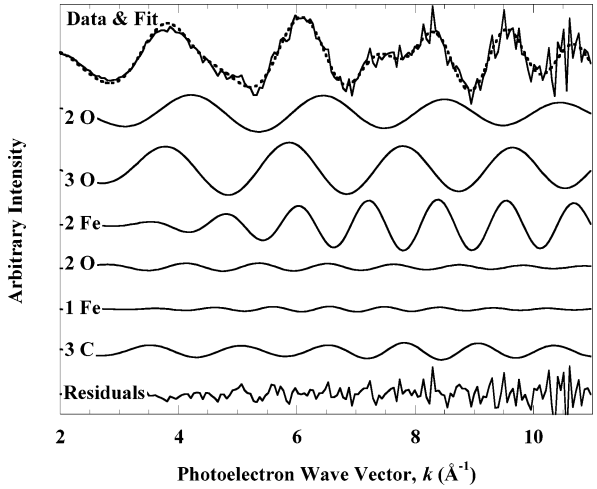

Figure 7. Fit to the iron K-edge EXAFS of *P. annectens* whole blood cells. Top: (—) EXAFS data; (- - -) fit to the EXAFS. Middle: (—) individual components to the fit. Each wave is labeled with the backscattering atom it represents. Bottom: (—) data minus fit residual. See Table 1 for the metrical details.

Table 1. EXAFS Fit Results

atom	CN	distance (Å)[a]	D−W (σ^2)	E_0 (eV)	F^b
O	2	1.93(1)	0.00393	−8.344	0.2476
O	3	2.07(1)	0.00233		
Fe	2	3.08(1)	0.00302		
O	2	3.29(7)	0.00731		
Fe	1	3.80(4)	0.01261		
C	3	2.87(2)	0.00230		

[a] Errors in distance are given in parentheses and represent the statistical uncertainty in the last digit calculated by the fit. [b] The goodness-of-fit function minimized was $F = [\sum k^6(\chi_{exptl} - \chi_{calcd})^2/\sum k^6\chi_{exptl}^2]^{1/2}$, where k is the photoelectron wave vector in $Å^{-1}$ and χ is the calculated or experimental EXAFS.

3.8-Å Zn reiterates the identity of the distant scatterer as a transition metal.

As noted previously, in the absence of further XAS data, the simplest model assumed an all-Fe cluster. The FT of the fit to the EXAFS data in terms of this model is shown in Figure 6, and the EXAFS data, the fit, and the components of the fit are shown in Figure 7. In all, a total of 72 different structural models were tested in these EXAFS fits, and the coordination numbers, distances, and DW values of the final fit are gathered in Table 1.

The structural models corresponding with the fit to the EXAFS were chosen by comparing the fit parameters with Fe−oxo or Fe−alkoxido complexes of known crystal structures including, but not limited to, Fe_3O_3 cyclohexanes and four-Fe cuboid structures featuring oxo or alkoxido ligands or bridges. Two-Fe dimers were eliminated because they are inconsistent with multiple second-shell Fe atoms. Regular four-Fe models consisting of fused, corner-sharing $[Fe_3O_4(OR)_n]$ diamond-core dimers were eliminated because they would not contain a 3.8-Å Fe−Fe vector (see Table 1) and did not produce a fit to the 3.4-Å FT feature.

In considering the choice of bridging groups, the 1.84−1.92-Å Fe−O distances known to typify oxo-bridged iron complexes[38] are shorter than the first-shell Fe−O distances found in the fits, making oxo-bridged irons unlikely. However, alkoxido-liganded polynuclear iron complexes proved to have Fe−Fe and Fe−O distances similar to those of the EXAFS fit (Table 2 in the Supporting Information). Alkoxide Fe−$OR_{terminal}$ distances range from 1.77 to 2.02 Å, and typically fall near ∼1.90 ± 0.05 Å. Likewise, Fe−$OR_{bridging}$ distances range over 1.84−2.08 Å and predominate in the region of ∼1.97 ± 0.05 Å. These comparisons indicated that the two shorter Fe−O distances found in the EXAFS fits best corresponded to terminal alkoxido ligands, and the three longer Fe−O distances to bridging alkoxido ligands.

Further comparisons showed that Fe_3O_3 metallocyclohexanes included 3.3−3.6-Å second-shell Fe−Fe distances,[39−41] which are longer than the 3.08-Å Fe−Fe distance found from the EXAFS fit (Table 1). However, the Fe−O and Fe−Fe distances in alkoxide-bridged Fe_3O_4 and Fe_4O_4 cubanes were again close to those found in the EXAFS fit (Table 2 in the Supporting Information). Fe^{III}−C_α distances in alkoxide complexes range over 2.8−3.0 Å,[42−44] which is also consistent with the 2.87-Å second-shell C atom found in the fit.

A perfectly regular Fe_4O_4 cubane would show three second-shell Fe scatterers at only one Fe−Fe distance. However, the best fits to the EXAFS found only two Fe−Fe scatters at 3.08 Å, and this distance is consistent with an alkoxido-bridged cubane. The more distant third iron at 3.8 Å completes the triad of Fe scatterers required of a cubane, but the long distance necessitates a further accounting. The mixed-valence polycubiodal iron complex $[Fe^{III}_4Fe^{II}_8(O)_2(OMe)_{18}(OAc)_6(MeOH)_{4.67}]$ includes four internal and slightly irregular Fe_4O_4 methoxide-bridged cubes that exhibit 16 Fe−Fe distances ranging between 3.09 and 3.30 Å, but with the lower end of this range predominating.[45] Thus, the 3.8-Å Fe−Fe distance of the EXAFS fit implies a structural distortion in a cubane model that cannot be accommodated by an unbroken Fe_4O_4 rectangular prism. This leads to an $Fe_4(OR)_4$ cuboidal model featuring one edge flared to produce a 3.8-Å Fe−Fe distance. The model includes two 3.8-Å Fe−Fe vectors, and the somewhat high DW value for this shell (Table 1) could signify a static spread of distances. The DW value is also similar to values found in EXAFS fits to similarly distant metal shells in some other complex clusters.[37,46]

Figure 8 shows two $[Fe_4$-μ-$(OR)_4]$ models as solutions to the distances and coordination numbers found in the best EXAFS fit and the overall structural considerations described

(38) Que, L., Jr.; Tolman, W. B. *Angew. Chem., Int. Ed.* **2002**, *41*, 1114−1137.
(39) Drueke, S.; Wieghardt, K.; Nuber, B.; Weiss, J.; Bominaar, E. L.; Sawaryn, A.; Winkler, H.; Trautwein, A. X. *Inorg. Chem.* **1989**, *28*, 4477−4483.
(40) Sessler, J. L.; Sibert, J. W.; Burrell, A. K.; Lynch, V.; Markert, J. T.; Wooten, C. L. *Inorg. Chem.* **1993**, *32*, 4277−4283.
(41) Zheng, H.; Zang, Y.; Dong, Y. H.; Young, V. G.; Que, L., Jr. *J. Am. Chem. Soc.* **1999**, *121*, 2226−2235.
(42) Shoner, S. C.; Power, P. P. *Inorg. Chem.* **1992**, *31*, 1001−1010.
(43) Caneschi, A.; Cornia, A.; Fabretti, A. C.; Gatteschi, D.; Malavasi, W. *Inorg. Chem.* **1995**, *34*, 4660−4668.
(44) Burger, J.; Klufers, P. *Z. Anorg. Allg. Chem.* **1996**, *622*, 1740−1748.
(45) Taft, K. L.; Papaefthymiou, G. C.; Lippard, S. L. *Inorg. Chem.* **1994**, *33*, 1510−1520.
(46) Cinco, R. M.; McFarlane Holman, K. L.; Robblee, J. H.; Yano, J.; Pizarro, S. A.; Bellacchio, E.; Sauer, K.; Yachandra, V. K. *Biochemistry* **2002**, *41*, 12928−12933.

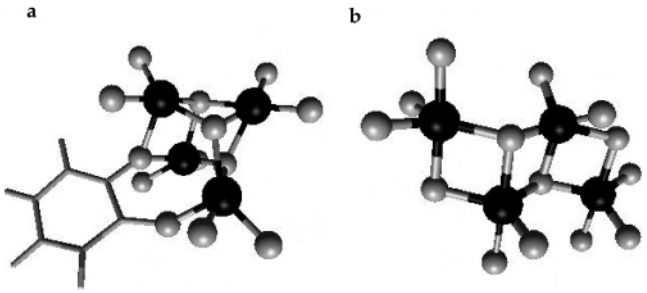

Figure 8. (a) Broken-edge cuboidal and, (b) Jacob's ladder structural representations of two alternative core $[Fe_4\text{-}\mu\text{-}(OR)_4]$ models for iron in *P. annectens* as deduced from the fit to the iron K-edge EXAFS spectrum. The first-shell Fe−O distances and second-shell Fe−Fe distances are all within ±0.02 Å of the scale of the EXAFS fit. The third-shell Fe−Fe distances, scaled to 3.8 ± 0.1 Å, are transverse across the open faces of the cuboid in part a or transverse across the μ_3-O in part b. Each Fe is five-coordinate, and all of the bridging and terminal ligands are to be alkoxides; however, the C atoms have been left out for clarity. The open face of the cuboid in part a is shown bridged by analogy with a known structural subunit (see Figure 10 in the Supporting Information), but the rationale for the choice of a bridging catecholate rests only on the DOPA- and TOPA-like molecules known to be ubiquitous in ascidians.[65,71]

above. Each model was constructed to the scale of the EXAFS fit distances. The first model depicts a broken-edge cuboid featuring two flared faces produced by disrupting one of the $Fe-OR_{bridging}$ edges to accommodate insertion of a new exogenous $Fe-OR_{terminal}$ bond. This structure averages two $Fe-OR_{terminal}$ interactions at 1.93 Å and three $Fe-OR_{bridging}$ interactions at 2.07 Å, as found in the EXAFS fit. Two transverse Fe−Fe distances occur at 3.08 Å, and there is one net Fe−Fe at 3.8 Å, again as required by the EXAFS fit. This broken-edge arrangement appears to be the most straightforward solution to the structurally challenging EXAFS results because, apart from the correct distances, it also includes the cubic motif suggested by the resemblance of the *P. annectens* iron K-edge XAS to that of magnetite.

A search of the structural literature located $[Fe_{10}(\mu_4\text{-}O)_3(\mu_3\text{-}O)_3(\mu_3\text{-}N,N\text{-diethylcarbamato-}O,O,O')(\mu_2\text{-}N,N\text{-diethylcarbamato})_6Cl]$.[47] This complex includes a component featuring an Fe^{III} cuboid with a structurally analogous broken edge that accommodates an extra carbamato O ligand, producing two 3.6-Å Fe−Fe distances. The relevant portion of this complex is shown for comparison in Figure 10a in the Supporting Information.

However, an alternative "Jacob's ladder" multinuclear iron structure was also found during the structural data search.[48−50] A model based on this structure, again scaled to the EXAFS distances, is shown in Figure 8b. The structurally analogous core of a known small molecule complex is shown in Figure 10b in the Supporting Information. This model averages two and a half Fe−O bonds of 1.93 and 2.07 Å each, with one and a half rather than two 3.08-Å Fe−Fe distances and one 3.8-Å Fe−Fe distance. These parameters produced an equally good fit to the EXAFS data, but with unrealistically low DW values both for the 2.07-Å Fe−O interaction ($\sigma^2 = 0.00142$) and for the second-shell 3.08-Å Fe−Fe interaction ($\sigma^2 = 0.00167$). This model also includes a 6.1-Å Fe−Fe distance that does not appear in the FT of the EXAFS data. Although it is possible to resolve EXAFS scatterers 6 Å away,[37,51−53] a rigid structure is generally required along with a back-scattering path that is either clear line-of-sight or with a dihedral angle near 180° and intermediate focusing atoms. However, static disorder in relative positions can readily wash out distant EXAFS interactions. Thus, while the "Jacob's ladder" model does not as accurately meet the EXAFS fit criteria and has marginal DW values, it cannot be entirely excluded. A choice among models will require EXAFS data over a greater *k* range that could resolve possibly more distant Fe−Fe interactions imposing additional modeling constraints.

Discussion

The results reported here conclusively eliminate the possibility that any significant fraction of the iron in *P. annectens* is dissolved in aqueous solution, despite the reported acid reaction of whole blood.[5] Clearly, however, the most pressing question to resolve in this study is whether the iron detected by XAS in *P. annectens* reflects one major complex, is the average of many complexes, or is an artifact of adventitious iron. The only sure test is to isolate an iron complex in pure form from *P. annectens* followed by an XAS measurement. Although this surety is currently absent, other inferences are available from the present data. First, the same iron K-edge XAS spectrum was consistently obtained from both whole-body and whole-blood-cell samples. This indicates that whatever alternative or artifactual iron may be present in nonhemolymphic tissues either is identical with the iron composition of the blood cells or contributes only a minor fraction of the total iron. Second, the variations noted in the XAS spectra among the independently collected whole-body and whole-blood-cell samples were far more consistent with redox activity in a single type of iron than with two or more large pools of dissimilar iron in *P. annectens*. The differences between the two independent whole-body XAS spectra (Figure 4) are much smaller, for example, than differences between the XAS spectra of the diferric and semireduced forms of the Fe_2O_2 iron site of MMO[36] or between the iron K-edge XAS spectra of Fe_2O_3 and Fe_3O_4.[54,55] If these independent *P. annectens* samples contained significant concentrations of multiple forms of iron, then the observed modest differences reflected in the XAS

(47) Dell'Amico, D. B.; Boschi, D.; Calderazzo, F.; Ianelli, S.; Labella, L.; Marchetti, F.; Pelizzi, G.; Quadrelli, E. G. F. *Inorg. Chim. Acta* **2000**, *300*, 882−891.
(48) Grant, C. M.; Knapp, M. J.; Streib, W. E.; Huffman, J. C.; Hendrickson, D. N.; Christou, G. *Inorg. Chem.* **1998**, *37*, 6065−6070.
(49) Seddon, E. J.; Yoo, J.; Folting, K.; Huffman, J. C.; Hendrickson, D. N.; Christou, G. *J. Chem. Soc., Dalton Trans.* **2000**, 3640−3648.
(50) Ammala, P.; Cashion, J. D.; Kepert, C. M.; Moubaraki, B.; Murray, K. S.; Spiccia, L.; West, B. O. *Angew. Chem., Int. Ed.* **2000**, *39*, 1688−1690.
(51) Liu, H. I.; Burgess, B. K.; Natoli, C. R.; Filipponi, A.; Gavini, N.; Hedman, B.; Di Cicco, A.; Hodgson, K. O. *J. Am. Chem. Soc.* **1994**, *116*, 2418−2423.
(52) Gailer, J.; George, G. N.; Pickering, I. J.; Prince, R. C.; Kohlhepp, P.; Zhang, D.; Walker, F. A.; Winzerling, J. J. *J. Am. Chem. Soc.* **2001**, *123*, 10121−10122.
(53) Corbett, M. C.; Hui, Y.; Naderi, F.; Ribbe, M. W.; Hedman, B.; Hodgson, K. O. *J. Biol. Chem.* **2004**, *279*, 28276−28282.
(54) Li, S.; Meitzner, G. D.; Iglesia, E. *J. Phys. Chem. B* **2001**, *105*, 5743−5750.
(55) Nichol, H.; Gakh, O.; O'Neill, H. A.; Pickering, I. J.; Isaya, G.; George, G. N. *Biochemistry* **2003**, *42*, 5971−5976.

spectra would imply nearly invariant ratios of iron distributed among all of the purportedly dissimilar pools. This coincidence seems unlikely, and is not found, for example, in the ratios of vanadium types in blood cells from independent samples of the tunicate *P. nigra*, as reflected in vanadium K-edge XAS spectra.[8] Third, the similarity in XAS spectra of magnetite and *P. annectens* iron, especially in the first-derivative spectra, requires another unlikely coincidence if the latter derives from a mixture of iron types. Fourth, the large second-shell iron peak in the *P. annectens* FT EXAFS spectrum is consistent only with an organized multinuclear metal site. This strengthens inference three, namely, that the similarity with the iron K-edge of magnetite reflects a coherent Fe site somehow analogous to an Fe_4O_4 cubane.

We further note here that the K-edge XAS FT spectrum of iron in *P. annectens* is strikingly similar to that found for iron in an Fe−ZSM-5 zeolite catalyst, which data have been interpreted in terms of an Fe_4O_4 iron site.[56] Interestingly, the metrics of the zeolite cubane are also similar to those found for *P. annectens* iron, with Fe−O distances of 1.93 and 2.03 Å and an Fe−Fe distance of 3.00 Å, but notably lacking both the C feature at 2.11 Å and the high-*R* shoulder on the second FT peak arising from the distant Fe and O scatterers.

The results reported here could be confounded by possible iron artifacts that might arise in ascidians following consumption of iron-accumulating diatoms.[5] However, the uniformity of the iron XAS between whole blood cells and whole bodies argues against artifactual ingested iron. Whole blood cells should also have been free of any exogenous iron-containing concretions. The consistency of the XAS between the two independent whole-body samples implies a similar conclusion.

In other iron-accumulating tunicates, iron is overwhelmingly localized in blood cells and often associated with cell membranes,[57,58] consistent with a majority single iron type. The gene for the iron-storage protein ferritin has recently been identified in the vanadium-concentrating ascidian *A. sydneiensis samea*.[59,60] However, the iron K-edge XAS (Figure 5) and FT EXAFS (Figure 8 in the Supporting Information) of ferritin are very dissimilar from those of *P. annectens* iron, eliminating ferritin iron as a major component of the biological iron in this species. Likewise the intense feature at 3 Å in the FT spectrum of magnetite (Figure 9 in the Supporting Information) eliminates this material as a confounding contaminant in the *P. annectens* samples. The consistency of the *P. annectens* XAS data is thus most reasonably understood as a single type of iron. Although other forms of iron are possibly present, they are also likely to be only a minor fraction of the total iron and to not contribute significantly to the XAS spectrum.

We next discuss the biological chemistry of the Fe site as revealed by the XAS study and finish with the biological import of the work. No matter which model proves to represent the Fe site, or an unanticipated third structure, it is nevertheless clear that a new multinuclear motif for biological iron resides in *P. annectens* blood cells.

As described above, the choice of alkoxido ligands to iron follows from an analysis of the Fe−O bond lengths. Small-molecule monobridging Fe^{III}−O carboxylates apparently remain unknown, which obviates an assessment of this alternative bridging mode. However, terminal Fe^{III}−O carboxylate bonds range over 1.97−2.06 Å.[61−64] Assignment of the 2.07-Å EXAFS distance to a terminal carboxylate leaves the 1.93-Å distance too long for the typical Fe^{III} μ-$(O)_2$ bridge but too short for a μ-$(OH)_2$ bridge and likewise leaves the 3.08-Å Fe−Fe distance too long for a μ-oxo-bridged Fe site[38] The alternative and more likely assignment of the 2.07-Å distance to the bridging Fe−O then eliminates carboxylate as a terminal ligand. This again leaves alkoxide as the preferred choice for both bridging and terminal ligands.

The best formula for the multinuclear site, including four five-coordinate Fe atoms with bridging and terminal alkoxide ligands, is $[Fe_4(OR)_{13,14}]^{-/2-}$ as shown in Figure 8. For reasons related to the EXAFS fit criteria noted above, we currently favor the broken-edge cuboid model (Figure 8a) over the "Jacob's ladder" model (Figure 8b) as the best hypothesis for this Fe site. Iron- and vanadium-accumulating ascidians are known to be enriched in a variety of phenolic metabolites[58,65,66] and in DOPA-containing polypeptides.[67,68] Likewise, the protein ferreascidin, first isolated from the iron-concentrating ascidian *Pyura stolonifera*,[69,70] includes a large number of DOPA units derived from post-translational modification. Phenolic or catecholic groups are thus the preferred hypothetical choice for the alkoxido ligands to iron. Ferreascidin assembles bi- and trinuclear Fe sites when exposed to iron in vitro.[70,71] A protein in *P. annectens* similarly equipped with phenolic residues would be a likely candidate to contain the Fe core described here. This protein may be membrane-bound (see below).

(56) Joyner, R.; Stockenhuber, M. *J. Phys. Chem. B* **1999**, *103*, 5963−5976.
(57) Agudelo, M. I.; Kustin, K.; Robinson, W. E. *Comp. Biochem. Physiol.* **1982**, *72A*, 161−166.
(58) Agudelo, M. I.; Kustin, K.; McLeod, G. C.; Robinson, W. E.; Wang, R. T. *Biol. Bull.* **1983**, *165*, 100−109.
(59) Yamaguchi, N.; Togi, A.; Ueki, T.; Uyama, T.; Michibata, H. *Zool. Sci.* **2002**, *19*, 1001−1008.
(60) Yamaguchi, N.; Kamino, K.; Ueki, T.; Michibata, H. *Mar. Biotechnol.* **2004**, *6*, 165−174.
(61) Thich, J. A.; Ou, C. C.; Powers, D.; Vasiliou, B.; Mastropaolo, B.; Potenza, J. A.; Schugar, H. J. *J. Am. Chem. Soc.* **1976**, *98*, 1425−1433.
(62) Shweky, I.; Bino, A.; Goldberg, D. P.; Lippard, S. J. *Inorg. Chem.* **1994**, *33*, 5161−5162.
(63) Goodwin, J. C.; Sessoli, R.; Gatteschi, D.; Wernsdorfer, W.; Powell, A. K.; Heath, S. L. *J. Chem. Soc., Dalton Trans.* **2000**, 1835−1840.
(64) Schmitt, W.; Anson, C. E.; Pilawa, B.; Powell, A. K. *Z. Anorg. Allg. Chem.* **2002**, *628*, 2443−2457.
(65) Parry, D. L.; Brand, S. G.; Kustin, K. *Bull. Mar. Sci.* **1992**, *50*, 302−306.
(66) Kim, D. S.; Li, Y. Y.; Horenstein, B. A.; Nakanishi, K. *Tetrahedron Lett.* **1990**, *31*, 7119−7122.
(67) Taylor, S. W.; Ross, M. M.; Waite, J. H. *Arch. Biochem. Biophys.* **1995**, *324*, 228−240.
(68) Taylor, S. W.; Craig, A. G.; Fischer, W. H.; Park, M.; Lehrer, R. I. *J. Biol. Chem.* **2000**, *275*, 38417−38426.
(69) Taylor, S. W.; Chase, D. B.; Emptage, M. H.; Nelson, M. J.; Waite, J. H. *Inorg. Chem.* **1996**, *35*, 7572−7577.
(70) Taylor, S. W.; Cashion, J. D.; Brown, L. J.; Hawkins, C. J.; Hanson, G. R. *Inorg. Chem.* **1995**, *34*, 1487−1494.
(71) Taylor, S. W.; Kammerer, B.; Bayer, E. *Chem. Rev.* **1997**, *97*, 333−346.

A comparison of *P. annectens* blood-cell iron XAS with the K-edge XAS spectra of magnetite and the numerically generated spectrum of partially reduced MMO showed that the iron in the blood cells and bodies of the collection 1 *P. annectens* samples was approximately 33% Fe^{II}. A similar comparison with the first-derivative XAS spectrum of the whole-body sample of collection 2 (data not shown) indicated about 40% Fe^{II} in this sample, clearly implying redox activity and reinforcing the conclusions drawn from the XAS spectral comparison in Figure 4. In the proposed four-Fe cluster, the apparent net valence change of $-0.07e^-$ observed between the collection 1 and 2 whole-body samples is equivalent to 28% reduction of a single Fe site. The redox molecular orbital in an O-bridged four-Fe cluster may be extensively delocalized, and upon one-electron reduction, the iron XAS spectrum is likely to reflect the continuing Fe^{III}/Fe^{II} mixed-valence character of the cluster. The change in iron XAS per electron transferred is then expected to be less than that observed for a mononuclear Fe site. The energy shifts in the rising-edge p-symmetry features with a single-electron redox of a tetrameric Fe site will also be smaller than the large redox-induced changes of a mononuclear Fe site because the change in the Z_{eff} per iron will reflect only about 0.25 electron. This appears to be what is observed in the rising K-edge spectra and first derivatives of the XAS spectra of *P. annectens* iron, where the characteristic features remain through a moderate redox change.

The situation governing the preedge features arising from the redox-active 3d valence orbitals appears slightly different, however. In simple octahedral monomeric and dimeric iron complexes, a one-electron reduction decreases the preedge intensity by 10−20%, expressed as $[(I_{Fe^{3+}} - I_{Fe^{2+}})/I_{Fe^{3+}}]$ (where I = pseudo-Voigt-fitted intensity).[19] The analogous intensity change for *P. annectens* whole-body collections 1 and 2, following a $0.28e^-$ reduction was $[(18.5 - 12.5)/18.5] = 0.32$. Dividing this value by 4 to account for iron nuclearity makes the per iron intensity change = 0.081, equivalent to an intensity decrease of 29% per electron per iron assuming a linear model. This value is greater than that reported for all of the ferrous/ferric octahedral models within a constant ligand environment but is smaller than the 38% decrease in the integrated preedge intensity for the tetrahedral complex $[FeCl_4]^{-/2-}$.[19] This result is explicable if the *P. annectens* iron is indeed noncentrosymmetric, as indicated by the XAS edge and EXAFS analyses above, but with less 3d−4p mixing than is typical of tetrahedral complexes.

The overall picture derived from iron K-edge XAS and EXAFS is then of a new cuboidal-core Fe_4O_5 iron site engaging in biological redox chemistry in *P. annectens*. Such a site may have an enzymatic role, and we note that the 3.8-Å Fe−Fe distance is consistent with the space requirements of bound small molecules.

A single-lobed transferrin, detected in the plasma of the ascidians *P. stolonifera* and *Halocynthia roretzi*,[72,73] along with the gene for ascidian ferritin[59,60] provides an experimental basis for the iron transport and storage metabolism required to support the Fe site described here. In the iron-containing ascidian *Styela clava*, dissolved Fe^{II} is directly taken up by blood cells, but ingested iron is acquired by this organism by capture of suspended particulates.[74] The majority of blood-cell iron in *A. dispar* and *P. chilensis* is in a soluble form and, in the latter ascidian, is associated with a protein.[75,76] However, in *Boltenia ovifera*, *S. clava*, and *Molgula manhattensis*, blood-cell iron is strongly associated with membranes, where it resists removal by 0.1 N HCl, and accounts for 70−90% of the total iron.[58] Blood lysates of these latter ascidians additionally include a minority of iron in soluble proteins. The K-edge XAS spectra of the iron in the blood cells of *P. annectens* are consistent with ∼90% dominance by a single form of iron, possibly analogous to the high proportion of membrane-associated iron in the above organisms. *P. annectens* iron thus may reflect a large enzymatic commitment to some discrete metabolic function.

A final major question arising from this work revolves around the change in the transition-metal content in *P. annectens*. The previous entirely credible metals report on this species presented duplicate blood-cell analyses, showing 8000 and 9000 ppm V and 940 ppm Fe in 1972 and 700−2000 ppm V in 1973.[5] The 1972 Fe/V ratio of ∼1:9 is almost the reverse of that found by MCA in 2002, as reported above. This peculiarity is increased by the fact that both the present and past collections were obtained from Monterey Bay, CA. Thus, there is no possibility of confusion with a different organism and no reason to suspect that the change in metal ratios reflected an environmental difference. Relatively high levels of vanadium were found in the blood cells of *P. viridis*, collected at Woods Hole, MA, in 1963,[15] implying that a higher vanadium but lower iron content typified the Perophoridae until recently. However, no systematic comparison of iron and vanadium has ever been carried out within this genus or within any other tunicate genus. It should also be noted that while we have not carried out phylogenetic analysis, *P. annectens* has a completely distinctive morphology not related to any other ascidian in the Monterey Bay area.[1]

The apparent shift from concentrating vanadium to concentrating iron thus remains very mysterious but has broad implications. First, it is not clear what physiological need is served by blood-cell metal in *P. annectens*, and thus the functional implications of the elemental change in stored metals are completely unknown.

Furthermore, the biological transporters that concentrate metals several million times above ambient levels are unknown. It is possible that multiple transporters with different metal specificities may exist in the genome and be selectively expressed, or there may be some plasticity to metal affinity of a single transporter. However, Blast searches

(72) Martin, A. W.; Huebers, E.; Huebers, H.; Webb, J.; Finch, C. A. *Blood* **1984**, *64*, 1047−1052.
(73) Abe, Y.; Nagata, R.; Hasunuma, Y.; Yokosawa, H. *Comp. Biochem. Physiol. B* **2001**, *128*, 73−79.
(74) Curtin, M. A.; Kustin, K.; Robinson, W. E. *Biol. Bull.* **1985**, *169*, 152−163.
(75) Roman, D. A.; Molina, J.; Rivera, L. *Biol. Bull.* **1988**, *175*, 154−166.
(76) Pizarro, J.; Andrade, C.; Crivelli, I. *Comp. Biochem. Physiol. A* **1989**, *94*, 777−781.

of the *Ciona intestinalis* and *C. savignyi* genomes (related ascidians with complete genome sequences) with cDNA and protein sequences of transporter proteins (e.g., the Na−K ATPase, Na/Cl cotransporter) do not reveal large gene families, despite the high conservation of these sequences across evolutionary time (not shown). Thus, we do not know how the apparent changeover from vanadium to iron is occurring or evolving or even whether the change is somatic or mutational, but the underlying physiology is bound to be exciting. Finally, following from the work reported here, and at the very least, vanadium domination of blood-cell metals cannot be taken as a defining trait of Phlebobranch tunicates so long as *P. annectens* is included among them.

Acknowledgment. This work was supported by Grant NIH RR-01209 (to K.O.H.). XAS data were collected at SSRL, which is supported by the Department of Energy, Office of Basic Energy Sciences. The SSRL Structural Molecular Biology Program is supported by the National Institutes of Health, National Center for Research Resources, Biomedical Technology Program, and by the Department of Energy, Office of Biological and Environmental Research.

Supporting Information Available: Tables of the test results of low-*Z* scatterers and selected distances for Fe^{III}−O alcoholate complexes and figures of various MCA, XAS, and EXAFS spectra and known structural precedents for the proposed models of *P. annectens* blood-cell iron. This material is available free of charge via the Internet at http://pubs.acs.org.

IC051445X